Conceptual Design and Sensitivity Analysis of MRI Magnets From REBCO HTS Tapes

Yakup Boran, Husnu Kara, Fedai Inanir, and Sukru Yildiz

***Abstract*—An actively shielded wide-bore magnet system has been designed for magnetic resonance imaging. The gradient-based optimization solver of COMSOL Multiphysics has been used to obtain an optimum geometrical arrangement of symmetrical electromagnets in the magnetic resonance imaging (MRI) system. To generate a high and homogeneous magnetic field, we employed a second-generation rare-earth barium-copper-oxide (REBCO) high-temperature superconductor (HTS), which was wound into 10 double pancake coils (DPC). The dimensions of the DPC sets have been chosen considering the size of REBCO HTS tapes, and the optimized design solution provides magnetic field, stray field, and current passing through the HTS tapes on each DPC set. The design details of a 1.5 T actively shielded magnet as well as the sensitivity analysis of the inhomogeneity, stray field, and currents with respect to coil positions have been presented. Optimum parameters for various designs are listed. The inhomogeneity of 1.23 ppm in the 200 mm diameter of spherical volume (DSV) and a stray field of as low as 0.05 G outside of the 5 m distance were achieved. Additionally, a low peak field of 2.40 T in DPC sets has been accomplished.**

***Index Terms*—COMSOL, double pancake coil, high temperature superconductor, magnetic resonance imaging.**

I. Introduction

SINCE the first magnetic resonance imaging (MRI) devices were built in 1970, an enormous amount of work has been done to improve MRI technology. Today, MRI holds great promise for progress in medical imaging and treatment of the human body. Approximately half a million MRI scans are performed worldwide every day [1]. Investment in MRI devices is predicted to grow even more in the future in order to improve image quality and meet increasing treatment demands [2], [3]. It is possible to design and fabricate MRI magnets with superconducting magnets, permanent magnets, and resistive magnets. Due to the limitations imposed by resistive and permanent magnets, especially in the context of field strength, superconducting magnets are commonly used. Superconducting magnets also have very low operating power when compared to resistive and permanent magnets [4]. There are two types of MRI magnets: the first is unshielded magnets with stray fields greater than 100 G, which can damage electronic devices placed near the magnet [5]. The second is shielded magnets, which have a stray field of approximately 5 G at a certain distance [6]. Shielding can be achieved through the use of ferromagnetic materials or coils carrying current in reverse directions [7]. The MRI superconducting magnet is the key element of MRI systems. Some of the MRI main magnets used today are wound with low temperature superconductor niobium-titanium (NbTi), which has a critical temperature of 9.2 K [8]. To improve the current capacity of the NbTi wires, the magnets are cooled down to temperatures far below the critical temperature of 9.2 K using a liquid helium (LHe) bath [9]. Most of the MRI systems require approximately 2000–3000 L of LHe to be cooled and operated over their lifetime [10]. Considering this situation, the amount of helium required to cool all of the world's MRI magnets is quite large. As a result of this scenario, MRI magnet technology is evolving into systems that use little or no helium. Recently, new technologies, such as Philips Ingenia Ambition, have become available that use microcooling systems requiring $\sim$7 L of LHe [11], but these systems are still not LHe-free. One noteworthy technology in this context is the cryostat technology with conduction cooling. This technology does not require the bath system that reduces the cost of cooling, hence, the operating cost [12]. Another, and possibly the best, alternative to conduction cooling technology is high temperature superconductor (HTS) based MRI magnet. These magnets are more convenient since they do not require helium cryogen [13]. In these systems, the superconducting magnets made by HTS tapes have the capability of carrying high electrical current density and, thus producing a sufficiently high magnetic field. Another benefit of using the HTS in MRI systems is that it reduces the weight and size, making MRI systems more compact with lower operation costs [14]. HTS-based MRI magnets were initially developed using Bi-2223 tape conductors, which performed admirably in terms of electromagnetic performance [15], [16]. The second generation (2G) rare-earth barium-copper-oxide (REBCO) HTS tape wound MRI magnet also showed an adequate magnetic field to be used in MRIs [17]. Sato et al. [15] designed MRI electromagnets that can produce 1.5 T magnetic field with 20 K conductor cooling using second

Manuscript received 12 April 2022; revised 30 July 2022; accepted 15 August 2022. Date of publication 22 August 2022; date of current version 30 August 2022. This paper was recommended by Associate Editor M. Parizh. *(Corresponding author: Yakup Boran.)*

Yakup Boran is with the Department of Engineering Fundamental Sciences, Sakarya University of Applied Sciences, 54187 Sakarya, Turkey (e-mail: yakupboran@subu.edu.tr).

Husnu Kara is with the Department of Basic Sciences, Necmettin Erbakan University, 42090 Konya, Turkey, and also with the Department of Physics, Yildiz Technical University, 34220 Istanbul, Turkey (e-mail: husnukara@erbakan.edu.tr).

Fedai Inanir is with the Department of Physics, Yildiz Technical University, 34220 Istanbul, Turkey (e-mail: inanir@yildiz.edu.tr).

Sukru Yildiz is with the Department of Metallurgical and Materials Engineering, Ahi Evran University, 40100 Kırşehir, Turkey (e-mail: sukru.yildiz@ahievran.edu.tr).

Color versions of one or more figures in this article are available at https://doi.org/10.1109/TASC.2022.3200575.

Digital Object Identifier 10.1109/TASC.2022.3200575

generation YBCO DPCs. Since the MRI magnet is an essential part of MRI systems, the volume of the MRI magnet utilized in MRI systems dominates the cost [6], so HTS tapes could be the best choice in designing MRI magnet. To obtain high image quality, MRI magnets should produce a uniform magnetic field of homogeneity at a level of 10 ppm in diameter of spherical volume (DSV). The level of stray field is also another criterion of MRI systems for public health safety consideration. A magnetic field of 5 G is usually sufficient to meet safety requirements [18]. In addition to magnetic field uniformity and stray field, quench protection and strain development studies are also important parts of the magnet design which are required to prevent damage to the magnet [19], [20].

In this article, using DPC, the optimal design of the superconducting main magnet and the shielding coil by the use of most common REBCO 2G HTS tape dimensions is presented. The majority of HTS conductors are made in a tape shape. This tape conductor can be used to create a superconducting coil as a helical coil or as a series of pancake coils. When a helical coil is used, if any local damage occurs, the entire coil needs to be replaced, but in the case of a pancake coil, only the damaged pancake coil requires replacement. Additionally, the helical coil's shape is deformed more as a result of the sidewise bending [21]. For these reasons, the pancake technique is commonly preferred to produce HTS coils. At the center of the symmetrical MRI main magnet system, a 1.5 T magnetic field with an inhomogeneity lower than 10 ppm was provided in a spherical volume of 0.20 m in diameter, and the magnitude of the stray magnetic field was reduced to below 5 G at a distance of 5 m from the center of the magnet system. For this design, a 2-D axisymmetric model and a gradient-based optimization solution tool are used in COMSOL Multiphysics. In order to achieve the most suitable currents that pass through the HTS tapes on DPC pairs, the number of windings and the positions of the DPC sets were varied, and the results are presented in detail.

II. Magnet Design

Magnetic fields in MRI magnets must be strong, uniform, and stable. In whole body MRI magnets, a 1.5 T magnetic field is commonly used, so in this article, the magnet was designed to operate at the same magnetic field of 1.5 T. In MRI systems, the magnetic field inhomogeneity is mostly defined in terms of peak-to-peak variation over a DSV. The DSV value was chosen at 0.20 m in diameter and the desired inhomogeneity was below 10 ppm. The selected geometry was a selenoid design with an inner diameter of 0.7 m, so whole body could fit into it. The aim of this article is to optimize the geometry and currents in order to obtain a magnetic field strength of 1.5 T with a maximum inhomogeneity of 10 ppm in a 0.20 m DSV region in the center of the DPC blocks. In order to calculate the magnetic field in z-direction (B_z) at any arbitrary point, considering that the electric field E is equal to zero and the magnetic field B does not change with time, the following Maxwell equations are solved numerically by the COMSOL multiphysics:

$$\nabla \cdot \overrightarrow{B} = 0 \tag{1}$$

$$\nabla \times \overrightarrow{H} = \overrightarrow{J} \tag{2}$$

$$\overrightarrow{H} = \overrightarrow{B}/\mu. \tag{3}$$

Here, H is the magnetic field strenght and $\mu = \mu_r \mu_0$ is the permeability where μ_r is the relative permeability and μ_0 is the permeability of the vacuum. Equations (1) and (2) have been solved using the finite element method. During this solution, two boundary conditions are applied: the magnetic insulation boundary and the perfect magnetic conductor boundary. In the first boundary condition, the magnetic field has only a tangential component, such that the normal component remains zero. This can be explained as follows: The current can flow in the normal direction to cut perpendicular to J and parallel to B. The second boundary condition is the opposite of the first boundary condition. Here, the magnetic field has a normal component while the tangential component is zero. In this case, there is a mirror symmetry plane for the current. On the other hand, for optimization, the objective functions to be minimized are as follows:

$$\int_0^{L_0} (B_z - B_0)^2 dz \tag{4}$$

$$\int_0^{L_0} \left(\frac{dB_Z}{dz}\right)^2 dz \tag{5}$$

where $L_0 = 10\,\mathrm{cm}$ and $B_0 = 1.5\,\mathrm{T}$. Optimization is achieved with the sparse nonlinear optimizer algorithm on the COMSOL platform [16]. The following parameters are used for the optimization: The maximum element size is 5×10^{-3} m, the minimum element size is 2×10^{-5} m, the maximum element growth rate is 1.1, and the curvature factor is 0.2. Fig. 1(a) depicts our initial geometry with a 2-D axisymmetric model, which consists of three main magnet sets. The main magnets are made up of DPC sets. The first and second coil sets each have one DPC, while the third coil set has three DPC. It contains 10 pairs of DPC when the entire magnet system is considered. Fig. 1(b) shows the magnetic flux density distribution for the magnet design when initial parameters are used. As can be seen clearly, inside the DSV region, the magnetic field is 1.5 T. The maximum field in the DPC sets is 2.38 T. The thickness of each superconducting tape is represented by h_{SC} in this diagram. The total thickness of the magnet is calculated by multiplying the h_{SC} by the number of coil turns. w_{SC} represents the width of each superconductor. The inner radii of the first, second, and third DPC sets are shown with r_1, r_2, and r_3. Finally, the starting positions on the z-axis of the first, second, and third DPC sets are represented by z_1, z_2, and z_3, respectively. In Fig. 1, only one-quarter of the DSV circle is shown. The inhomogeneity level of the full circle is the same as that of the quarter circle.

III. Results and Discussion

A. Modeling and Optimization of MRI Magnet Without Shielding

In this section, we introduce our magnet design having a inhomogeneity lower than 10 ppm in the DSV region using only the main magnets. There was no shielding system in this design to reduce the stray field. Here, only the currents passing through the DPC sets were optimized, and other parameters such as the

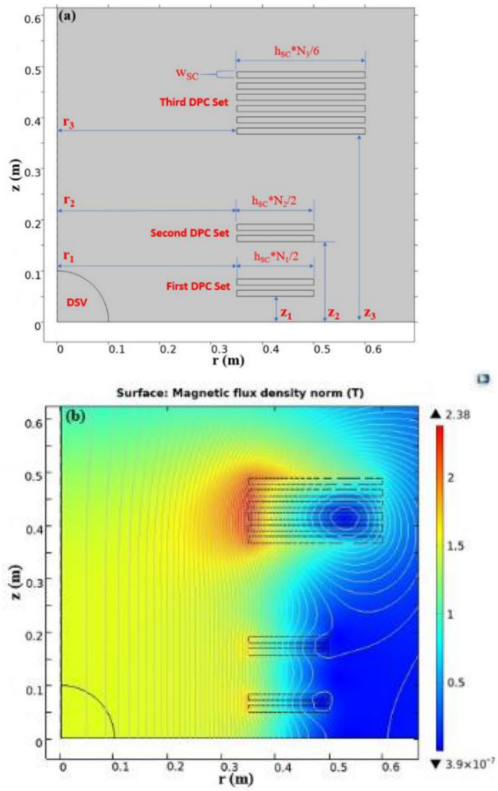

Fig. 1. 1.5 T magnet design. (a) Schematic representation of the magnet design showing the parameters. (b) Magnetic field profile of the magnet. Only one-quarter of the symmetric magnet and field profile is depicted.

TABLE I
INITIAL PARAMETERS OF MAGNET DESIGN WITHOUT SHIELDING DPC

Name(unit)	Value	Name(unit)	Value
r_1 (m)	0.35	h_{SC} (μm)	250
r_2 (m)	0.35	w_{SC} (mm)	12
r_3 (m)	0.35	dsv (m)	0.2
z_1 (m)	0.05	I_1 (A)	125.0
z_2 (m)	0.157	I_2 (A)	112.0
z_3 (m)	0.367	I_3 (A)	117.4
N_1	1200	InH (ppm)	2.31
N_2	1200	Stray field (G)	21.03
N_3	6000		

positions and the radii of the DPC sets were chosen arbitrarily. The initial parameters for the radius of each DPC set (r_1, r_2, and r_3), the axial position of each DPC set (z_1, z_2, and z_3), the number of turns for each DPC set (N_1, N_2, and N_3). The thickness (h_{SC}) and width (w_{SC}) are the dimensions of the HTS tapes. All the related values are provided in Table I. The inner diameter and outer diameter of the magnet system are 0.70 m and 1.20 m, and the length of the magnet system is 0.978 m. The number of turns for the first, second, and third DPC sets is 1200, 1200, and 6000, respectively. The thickness (h_{SC}) of the HTS tape was chosen 250 μm, which is relatively thick and has the following advantages: the robust mechanical performance, the high current carrying capability, comparatively less sensitive to the anisotropic field dependence [11]. The width (w_{SC}) of the HTS tape was preferred as 12 mm due to its higher current

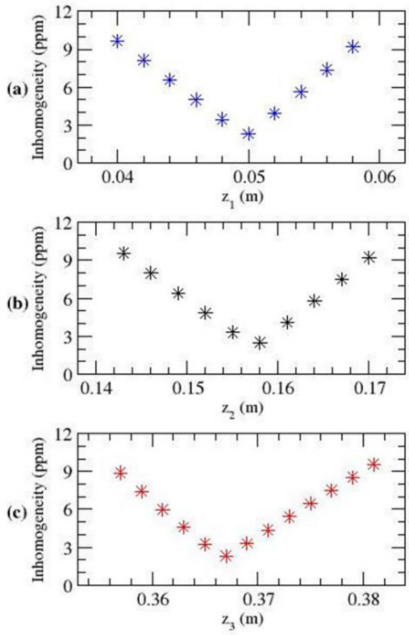

Fig. 2. Sensitivity of magnetic field inhomogeneity within the DSV of 20 cm with DPC axial positions without shielding DPC.

carrying capacity, and it has been widely fabricated at this size. Using these initial parameters, the currents passing through the HTS tapes for each DPC set (I_1, I_2, and I_3), inhomogeneity in the DSV region, and stray field 5 m outside the center of the MRI system were obtained. All these parameters are also given in Table I. Radial and axial parameters were varied with an increment of 0.1 mm to obtain a more realistic model that can be directly applied to the HTS magnet application.

The inhomogeneity in the DSV region with a diameter of 20 cm is 2.31 ppm, which is far below the desired 10 ppm value. I_1, I_2, and I_3 passing through the HTS tapes are 125 A, 112 A, and 117.4 A, which are also reasonable values for the HTS tapes since the current-carrying capacity of HTS tapes is reported up to 1000 A [13], [22]. The weakness of this design is the value of the stray field. The stray field at 5 m was found to be 21.03 G. For safety reasons, the stray field outside the MRI system room must be less than 5 G [2], [9]. These initial parameters do not meet the safety requirements. In order to reduce the stray field, the axial position and inner diameter of the DPC sets were varied. First, z_1 was varied between 0.04 m and 0.058 m, such that the inhomogeneity does not exceed 10 ppm, while z_2 and z_3 are kept at their initial values. The calculation was then repeated for the case where z_1 and z_3 remained constant and z_2 was altered between 0.143 m and 0.170 m. Finally, z_1 and z_2 were kept at their initial value, while z_3 was varied between 0.357 m and 0.381 m. The variation of the inhomogeneity and stray field with respect to axial positions of z_1, z_2, and z_3 are presented in Figs. 2 and 3. The results show that inhomogeneity is sensitive to axial positions, whereas the stray field is unlikely to be affected by axial positions. In each case, the inhomogeneity is decreased to around 2 ppm, but the stray field cannot be reduced below 20.72 G.

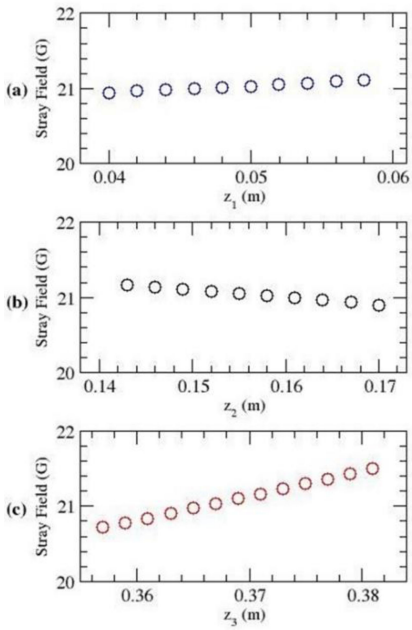

Fig. 3. Sensitivity of stray field on the 5 × 5 m region with DPC axial positions without shielding DPC.

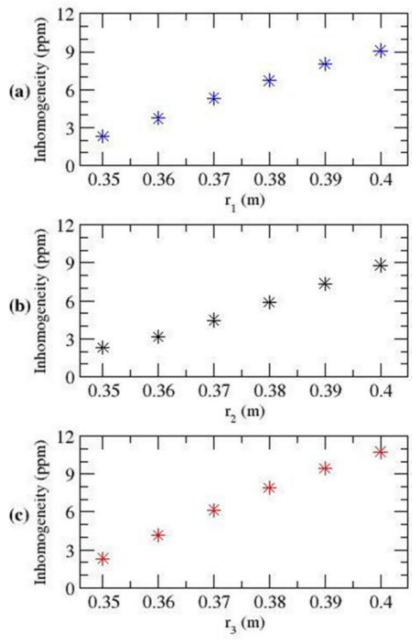

Fig. 4. Sensitivity of magnetic field inhomogeneity within the DSV of 20 cm with inner diameter of DPC without shielding DPC.

In the second part of the calculations, the inner radius of the DPC sets r_1, r_2, and r_3 were varied. Today, most MRI systems are commercially fabricated with a wide bore diameter (>60 cm). Since HTS tapes are wound around the gradient coil and RF coils, a 0.35 m inner radius was used to have at least a 60 cm bore diameter. In each case, the radius of one of the DPC sets was altered between 0.35 m and 0.40 m, while the radii of the other two DPC sets were kept at their initial value. Figs. 4 and 5 show

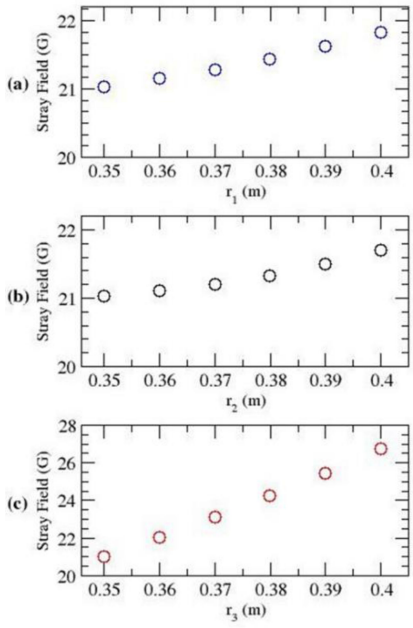

Fig. 5. Sensitivity of stray field on the 5 × 5 m region with inner diameter of DPC without shielding DPC.

how varying the radius of the coil sets affects inhomogeneity and stray field. As in the axial positions, the radius affects the inhomogeneity, but the radius has little effect on the stray field. The stray field was still around 21 G when r_1 and r_2 were varied from 0.35–0.40 m. Moreover, the stray field jumps to 26.72 G when r_3 was set to 0.40 m. As a result, increasing the radius also did not reduce the stray field to the desired value of 5 G. Varying the axial and radial positions of the coil sets did not lower the stray field. On the other hand, it can be concluded that since the inhomogeneity is lower than 10 ppm with different values of axial and radial positions, we have the opportunity to slightly change the magnet size. In order to reduce the stray field of magnet, the shielding method is used in most of the MRI systems. Shielding methods for high magnetic field devices are mainly classified into two types: passive shielding and active shielding [7]. Magnetic conductive materials are used in passive shielding to divert magnetic field lines around a region of interest. For a whole-body MRI system, passive shielding requires a large amount of conductive material to surround the MRI system, which is economically inconvenient [23]. On the other hand, active shielding uses secondary coils around the primary coils that produce magnetic fields in the opposite direction to suppress the magnetic field strength below 5 G around the MRI device and to achieve a homogenous magnetic field at the center of the MRI device. This makes the MRI device more compact and economic [24]. In the following section, the magnet design that has the shielding DPC will be discussed.

B. Modeling and Optimization of MRI Magnet With Shielding

The magnet design discussed in the previous section is not suitable to use in MRI systems since it does not satisfy the safety requirements of 5 G. The high stray field in a certain region is a

TABLE II
INITIAL PARAMETERS OF MAGNET DESIGN WITH SHIELDING DPC

Name(unit)	Value	Name(unit)	Value
r_1 (m)	0.35	h_{SC} (μm)	250
r_2 (m)	0.35	w_{SC} (mm)	12
r_3 (m)	0.35	dsv (m)	0.2
r_4 (m)	0.65	I_1 (A)	131.4
z_1 (m)	0.05	I_2 (A)	120.0
z_2 (m)	0.157	I_3 (A)	126.2
z_3 (m)	0.367	I_4 (A)	–50.0
z_4 (m)	0.455	InH (ppm)	2.89
N_1	1200	Stray field (G)	16.51
N_2	1200		
N_3	6000		
N_4	2000		

problem for this design. As mentioned previously, the shielding method can be employed to overcome this issue. A shielding DPC has been added to the magnet design that we discussed in the previous section. Since the shielding coil carries a current in the opposite direction that cancels the main field, it is aimed to reduce the stray field below 5 G with the shielding DPC. The design parameters are the same as the initial parameters listed in Table I. The shielding coil not only generates a magnetic field to offset the stray field of the primary coil but also adds an opposite magnetic field in the central area. Thus, it does not make sense to add the shielding coil directly to the optimized magnet design since the optimized profile will be perturbed significantly. Consequently, the optimization needs to be performed again [23]. When actively shielding coil is used, the optimum parameters for inhomogeneity, stray field, and currents are different from those in Table I. Therefore, initial parameters are provided again in Table II, including inhomogeneity, stray field, and currents for the magnet design with shielding DPC. In addition to Table I, the axial (z_4) and radial (r_4) positions of the shielding coil, number of turns (N_4) and current passing through the shielding coil (I_4) are added to Table II. The inner and outer diameters of the magnet system are 0.70 m and 1.8 m, respectively. While the number of turns for the main magnet DPC sets is the same as with the previous model, the number of turns for the shielding DPC is 2000, with 1000 turns on each coil. We first set the current on the shielding coil at –50 A to see the effect of the shielding. Using these initial parameters, the inhomogeneity in the DSV region is found to be 2.89 ppm, which satisfies the 10 ppm inhomogeneity condition. I_1, I_2, I_3 were obtained as 131.4 A, 120.0 A, and 126.2 A, respectively. These current values are all acceptable compared with the current carrying capacity of HTS tapes. When the shielding coil carries –50 A current, the stray field decreases from 21.03–16.51 G. In Fig. 6, the schematic of the magnet design and magnetic flux density of the same design in 2-D in the case of with shielding coil are shown.

In the presence of active shielding, the maximum magnetic field in the DPC sets is 2.44 T, which is very close to the maximum magnetic field of 2.38 T in the absence of shielding. This means that in both cases of with and without shielding, the currents on DPC sets will be almost the same, therefore, the magnet design with active shielding does not cause any concerns in DPC sets to produce the magnetic field of 1.5 T. Furthermore,

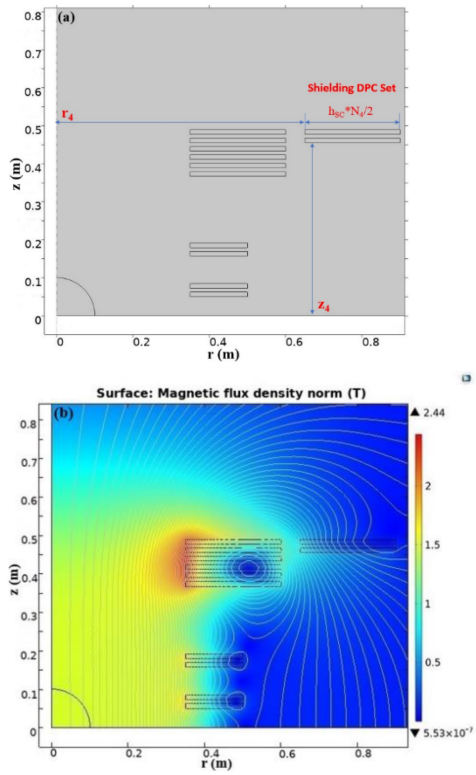

Fig. 6. 1.5 T magnet design. (a) Schematic representation of the magnet design including the shielding coil. (b) Magnetic field profile of the magnet with the shielding coil. Only one-quarter of the symmetric magnet and field profile is shown.

due to the low peak field at DPC sets, the magnet does not rapidly heat up to a damaging temperature, which is advantageous for quench protection [25]. Since we observed a positive effect on the stray field by adding a shielding DPC, the current flowing through it was varied to reduce the stray field. The current I_4 was altered between –50 A and –300 A. The effect of the I_4 on inhomogeneity, stray fields, as well as currents I_1, I_2, and I_3 was investigated. The results are shown in Fig. 7. The inhomogeneity increases with the increasing I_4, from 3 –6 ppm, which can be considered good enough to satisfy the 10 ppm condition.

On the other hand, the stray field was improved with the increasing I_4. The minimum stray field of approximately 0.15 G was obtained at around –230 A. The 5 G limit was observed at 2.13 m and 2.81 m in the radial and axial directions, respectively. The maximum field in the DPC sets was 2.65 T when a –230 A current was applied. The currents I_1, I_2, and I_3 increased by about 30% when I_4 was increased from –50 A to –300 A, but the results remained reasonable. The axial position and radial position of the shielding DPC were varied to see the variation of the stray field and inhomogeneity while the positions of the main DPC sets and the current on shielding DPC were kept constant. The current was chosen to be -230 A, which gives the minimum for the stray field. The radial (r_4) position of the shielding DPC was varied between 0.61 m and 0.69 m while axial position (z_4) was kept constant and currents on main DPC sets were optimized. As shown in Fig. 8, the inhomogeneity increased from 4.77–5.15 ppm, and the stray field was as low as 0.15 G at $r_4 = 0.65$ m. The

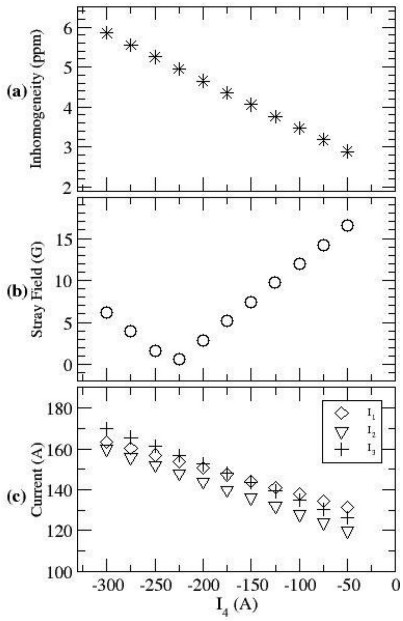

Fig. 7. Sensitivity of inhomogeneity, stray field and currents (I_1, I_2, and I_3) with shielding DPC. Stray field and inhomogeneity were measured at 5 m outside of the center of the MRI system.

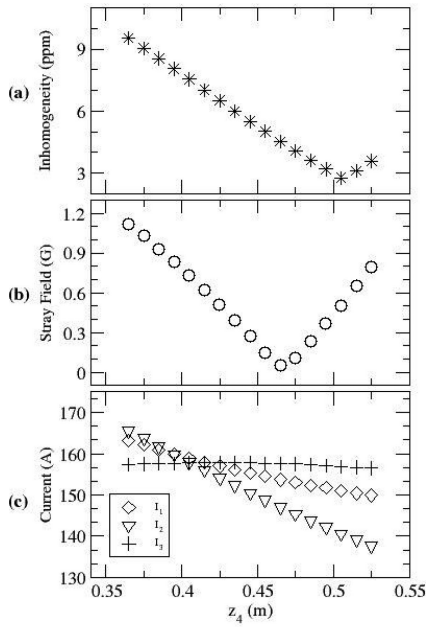

Fig. 9. Sensitivity of inhomogeneity, stray field and currents (I_1, I_2, and I_3) when position (z_4) of shielding DPC is varied. The current on shielding DPC is –230 A. Stray field and inhomogeneity were measured at 5 m outside of the center of the MRI system.

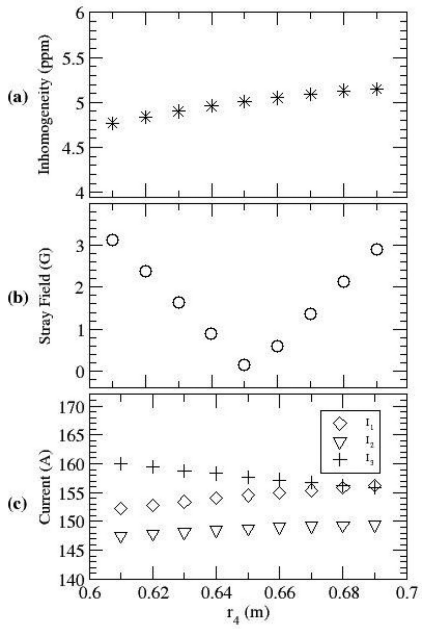

Fig. 8. Sensitivity of inhomogeneity, stray field and currents (I_1, I_2, and I_3) when radius (r_4) of shielding DPC is varied. The current on shielding DPC is –230 A. Stray field and inhomogeneity were measured at 5 m outside of the center of the MRI system.

change in r_4 increased the current on the first and second DPC while decreasing the current on the third DPC set. In Fig. 8, during the variation of r_4, the maximum current was around 160 A. It can be stated that the inhomogeneity, stray field, and currents on HTS tapes were all within reasonable limits. The axial position (z_4) of the shielding DPC was altered between 0.385 m and 0.525 m, while radial position (r_4) was held constant and currents on main DPC sets were optimized. As can be seen in Fig. 9, the best inhomogeneity (2.76 ppm) was obtained at around $z_4 = 0.505$ m, while the lowest stray field (0.05 G) was found at around $z_4 = 0.465$ m. The current I_1 reduced from 161–150 A, the current I_2 decreased from 162–138 A, while the current I_3 was not affected significantly as the axial position (z_4) of the shielding DPC changed. Here, it is worthwhile to mention that as z_4 gets larger, the magnet length increases. At $z_4 = 0.505$ m, a 45% improvement in inhomogeneity was achieved, at the expense of a 0.1 m increase in magnet length. Designers need to consider a harm-benefit balance at this point. When the z_4 is reduced from 0.455–0.405 m, the inhomogeneity increases from 5.01–7.54 ppm, while the stray field increases from 0.15–0.73 G. Following that, both the inhomogeneity and the stray fields increase with the decrease of z_4. In addition, since the third DPC and shielding DPC end at the same axial position, decreasing the z_4 does not affect the magnet size. As a result, reducing the z_4 does not provide any advantage.

Another investigation was to check whether the bore diameter of the magnet could be increased or not. The advantage of increasing the bore diameter is that the magnet will be more spacious, making patients feel more comfortable. In order to check this possibility, the radial parameters r_1, r_2, r_3, and r_4 were increased simultaneously while holding the axial positions (z_1, z_2, z_3, and z_4) and I_4 at –230 A. Keeping all other parameters constant and varying r_1, r_2, and r_3 from 0.35–0.40 m and r_4 from 0.65–0.70 m with an increment of 0.01 m results in inhomogeneity and stray field exceeding 10 ppm and 5 G limits. In order to reduce inhomogeneity, the axial positions of the DPC sets could be changed slightly. To optimize the stray field, the current I_4 could

TABLE III
OPTIMUM PARAMETERS FOR STRAY FIELD, INHOMOGENEITY, AND CURRENTS ON HTS TAPES FOR DIFFERENT RADII OF MAGNET WITH SHIELDING DPC

Name(unit)	A	B	C	D	E	F
r_1 (m)	0.35	0.36	0.37	0.38	0.39	0.40
r_2 (m)	0.35	0.36	0.37	0.38	0.39	0.40
r_3 (m)	0.35	0.36	0.37	0.38	0.39	0.40
r_4 (m)	0.65	0.66	0.67	0.68	0.69	0.70
z_1 (m)	0.05	0.05	0.05	0.05	0.05	0.05
z_2 (m)	0.157	0.1556	0.1564	0.1557	0.156	0.1562
z_3 (m)	0.3642	0.3717	0.3809	0.3888	0.3973	0.4057
z_4 (m)	0.4522	0.4597	0.4689	0.4768	0.4853	0.4937
I_1 (A)	148.5	147.4	147.1	145.9	145.0	143.9
I_2 (A)	137.3	143.8	152.0	159.4	167.5	175.7
I_3 (A)	147.9	153.2	158.5	164.0	169.4	174.9
I_4 (A)	-175.8	-187.9	-200.5	-213.1	-225.9	-239.0
InH (ppm)	2.68	2.29	1.90	1.66	1.42	1.23
Stray Field(G)	4.99	4.99	4.99	4.99	4.99	4.99
MF on DPC(T)	2.58	2.68	2.69	2.74	2.79	2.85

The letters from a to f present different magnet designs, having inner bore radii ranging 0.35 –0.40 cm.

be adjusted. In Table III, the optimum parameters for currents on HTS tapes for each DPC set, inhomogeneity, and stray field at the DSV region for different radii of magnets are provided. The results show that currents passing through the HTS tapes are all within the reasonable range of 137 A and 239 A. Inhomogeneity in the DSV region has the values from 2.68–1.23 ppm. The magnet design labeled as F requires 20% more current than the magnet design labeled as A. The maximum field on DPC sets is also all reasonable, ranging between 2.58 T and 2.85 T. The current on shielding DPC is approximately 25% of the total current of the magnet system for all magnet designs given in Table III. When active shielding is used, the total current of the magnet system increases, but since the persistent current mode is possible in REBCO HTS tapes, active shielding does not add any additional operation cost. We can conclude that increasing the bore diameter has a positive effect on inhomogeneity. Finally, the minimum stray field of 4.99 G was obtained and does not change after necessary optimizations are done. We can deduce that, at the expense of increasing the magnet's length by 9%, the bore diameter of the magnet could be increased by about 15%. As the results show, by using the COMSOL Multiphysics software, any magnet system with the desired length and bore diameter for different purposes could be designed that meets the safety requirements. Furthermore, a harm-benefit analysis could be performed to choose the best magnet parameters, i.e., decreasing current and increasing inhomogeneity up to a 10 ppm limit.

VI. CONCLUSION

A 1.5 T wide bore magnet for MRI systems has been designed. The magnet was composed of 10 pairs of main DPC sets to generate a homogeneous field and 2 pairs of shielding DPC sets to reduce the stray field. A uniform magnetic field suitable for MRI applications has been generated using the COMSOL multiphysics software. The stray field at certain distances has been adjusted to below safety limitations and the low peak field in DPC sets has been obtained. By varying different magnet parameters, unshielded, and actively shielded magnet designs have been optimized and the optimal parameters have been provided. For the cases with and without shielding DPC, the sensitivity of inhomogeneity and stray fields to the axial and radial positions of the DPC sets has been demonstrated. By using these results, the best inhomogeneity and stray field were obtained. We have proved that by varying the position of the DPC sets, it is possible to achieve 1.23 ppm of field inhomogeneity in a 0.20 m DSV region and a stray field of 0.05 G outside the 5 m. This low inhomogeneity provides a higher signal-to-noise ratio and, consequently, faster image collection, and better image quality. This means that diseases can be diagnosed and treated at earlier stages. Our results show that this MRI magnet design using REBCO HTS is suitable for use in clinical diagnosis and could be constructed. This sensitivity analysis could be considered effective and applicable for optimizing any proposed magnet design.

REFERENCES

[1] T. Baig, Z. Yao, D. Doll, M. Tomsic, and M. Martens, "Conduction cooled magnet design for 1.5 T, 3.0 T and 7.0 T MRI systems," *Supercond. Sci. Technol.*, vol. 27, 2014, Art. no. 125012.

[2] Y. Lvovsky, E. W. Stautner, and T. Zhang, "Novel technologies and configurations of superconducting magnets for MRI," *Supercond. Sci. Technol.*, vol. 26, no. 9, 2013, Art. no. 093001.

[3] Z. Wang, J. Oort, and M. Zou, "Development of superconducting magnet for high-field MR systems in China," *Physica C, Supercond.,* vol. 482, pp. 80–86, 2012.

[4] J. E. C. Williams, "Superconducting magnets for MRI," *IEEE Trans. Nucl. Sci.*, vol. 31, no. 4, pp. 994–1005, Aug. 1984.

[5] G. Sinha, R. Sundararaman, and G. Singh, "Design concepts of optimized MRI magnet," *IEEE Trans. Magn.*, vol. 44, no. 10, pp. 2351–2360, Oct. 2008.

[6] Z. Liang, "An optimal design of actively shielded MRI superconducting magnet," *IEEE Trans. Appl. Supercond.,* vol. 29, no. 2, Mar. 2019, Art. no. 4900404.

[7] B. Gastineau, C. Pes, and J. Ducret, "Comparison between active and passive shielding designs for a large acceptance superconducting dipole magnet," *IEEE Trans. Appl. Supercond.,* vol. 16, no. 2, pp. 485–488, Jun. 2006.

[8] D. Patel et al., "Niobium-titanium (Nb-Ti) superconducting joints for persistent-mode operation," *Sci. Rep.*, vol. 9, no. 1, 2019, Art. no. 14287.

[9] T. Baig et al., "Conceptual designs of conduction cooled MgB_2 magnets for 1.5 and 3.0 T full body MRI systems," *Supercond. Sci. Technol.*, vol. 30, no. 4, 2017, Art. no. 043002.

[10] C. Poole, T. Baig, R. J. Deissler, D. Doll, M. Tomsic, and M. Martens, "Numerical study on the quench propagation in a 1.5 T MgB_2 MRI magnet

design with varied wire compositions," *Supercond. Sci. Technol.*, vol. 29, no. 4, 2016, Art. no. 044003.

[11] Philips Ingenia Ambition 1.5T X MRI Scanner, Aug. 2018. [Online]. Available: https://www.USA.philips.com/healthcare/product/HC781356/ingenia-ambition-excel-in-your-daily-mr-services-helium-free

[12] M. S. Kim, S. Park, and Y. S. Choi, "Development of conduction-cooled cryostat for superconducting probe station," *IEEE Trans. Appl. Supercond.*, vol. 27, no. 4, Jun. 2017, Art. no. 0500505.

[13] B. Shen et al., "Development of an HTS magnet for ultra-compact MRI system: Optimization using genetic algorithm (GA) method," *IEEE Trans. Appl. Supercond.*, vol. 30, no. 4, Jun. 2020, Art. no. 4601805.

[14] S. Mukoyama et al., "Superconducting joint of REBCO wires for MRI magnet," *J. Phys., Conf. Ser.*, vol. 1054, 2018, Art. no. 012038.

[15] K.-I. Sato, S.-I. Kobayashi, and T. Nakashima, "Present status and future perspective of bismuth-based high-temperature superconducting wires realizing application systems," *Japanese J. Appl. Phys.*, vol. 51, 2012, Art. no. 010006.

[16] B. Parkinson, "Design considerations and experimental results for MRI systems using HTS magnets," *Supercond. Sci. Technol.*, vol. 30, no. 1, 2016, Art. no. 014009.

[17] S. Yokoyama et al., "Design and cooling properties of high stable field RE-BCO superconducting magnet for MRI," *IEEE Trans. Appl. Supercond.*, vol. 30, no. 4, Jun. 2020, Art. no. 4400904.

[18] K. Wu et al., "An optimized design approach for 14 T actively shielded MRI magnets," *IEEE Trans. Appl. Supercond.*, vol. 30, no. 4, Jun. 2020, Art. no. 4400504.

[19] R. J. Deissler et al., "Numerical simulation of quench protection for a 1.5 T persistent mode MgB_2 conduction-cooled MRI magnet," *Supercond. Sci. Technol.*, vol. 30, no. 2, 2016, Art. no. 025021.

[20] A. Amin et al., "A multiscale and multiphysics model of strain development in a 1.5 T MRI magnet designed with 36 filament composite MgB_2 superconducting wire," *Supercond. Sci. Technol.*, vol. 29, 2016, Art. no. 055008.

[21] A. Hekmati and R. Hekmati, "Double pancake superconducting coil design for maximum magnetic energy storage in small scale SMES systems," *Cryogenics*, vol. 80, pp. 74–81, 2016.

[22] H. Zhang, Z. Wen, F. Grilli, K. Gyftakis, and M. Mueller, "Alternating current loss of superconductors applied to superconducting electrical machines," *Energies*, vol. 14, 2021, Art. no. 2234.

[23] Y. Wang et al., "Actively-shielded ultrahigh field MRI/NMR superconducting magnet design," *Supercond. Sci. Technol.*, vol. 35, no. 1, 2021, Art. no. 014001.

[24] Z. Ni, G. Hu, L. Li, G. Yu, Q. Wang, and L. Yan, "Globally optimal algorithm for design of 0.7 T actively shielded whole-body open MRI superconducting magnet system," *IEEE Trans. Appl. Supercond.*, vol. 23, no. 3, Jun. 2013, Art. no. 4401104.

[25] A. Oraon, R. Oraon, S. Ghosh, S. Aich, and G. Sinha, "Simulation-Based design of optimized symmetric MRI magnet modified with ferromagnetic shell," *IEEE Trans. Magn.*, vol. 56, no. 2, Feb. 2020, Art. no. 8000207.